

Nuclear binding near a quantum phase transition

Serdar Elhatisari,¹ Ning Li,² Alexander Rokash,³ Jose Manuel Alarcón,¹ Dechuan Du,² Nico Klein,¹ Bing-nan Lu,² Ulf-G. Meißner,^{1,2,4} Evgeny Epelbaum,³ Hermann Krebs,³ Timo A. Lähde,² Dean Lee,⁵ and Gautam Rupak⁶

¹*Helmholtz-Institut für Strahlen- und Kernphysik and Bethe Center for Theoretical Physics, Universität Bonn, D-53115 Bonn, Germany*

²*Institute for Advanced Simulation, Institut für Kernphysik, and Jülich Center for Hadron Physics, Forschungszentrum Jülich, D-52425 Jülich, Germany*

³*Institut für Theoretische Physik II, Ruhr-Universität Bochum, D-44870 Bochum, Germany*

⁴*JARA - High Performance Computing, Forschungszentrum Jülich, D-52425 Jülich, Germany*

⁵*Department of Physics, North Carolina State University, Raleigh, NC 27695, USA*

⁶*Department of Physics and Astronomy and HPC² Center for Computational Sciences, Mississippi State University, Mississippi State, MS 39762, USA*

How do protons and neutrons bind to form nuclei? This is the central question of *ab initio* nuclear structure theory. While the answer may seem as simple as the fact that nuclear forces are attractive, the full story is more complex and interesting. In this work we present numerical evidence from *ab initio* lattice simulations showing that nature is near a quantum phase transition, a zero-temperature transition driven by quantum fluctuations. Using lattice effective field theory, we perform Monte Carlo simulations for systems with up to twenty nucleons. For even and equal numbers of protons and neutrons, we discover a first-order transition at zero temperature from a Bose-condensed gas of alpha particles (⁴He nuclei) to a nuclear liquid. Whether one has an alpha-particle gas or nuclear liquid is determined by the strength of the alpha-alpha interactions, and we show that the alpha-alpha interactions depend on the strength and locality of the nucleon-nucleon interactions. This insight should be useful in improving calculations of nuclear structure and important astrophysical reactions involving alpha capture on nuclei. Our findings also provide a tool to probe the structure of alpha cluster states such as the Hoyle state [1–6] responsible for the production of carbon in red giant stars and point to a connection between nuclear states and the universal physics of bosons at large scattering length [7, 8].

PACS numbers: 21.60.De, 21.10.Dr, 21.30.-x, 13.75.Cs, 67.10.Ba, 67.85.Jk

There have been significant recent advances in *ab initio* nuclear structure theory using a variety of different methods [9–15]. Much of the progress has been driven by computational advances, but we also have a better conceptual understanding of how nuclear forces impact nuclear structure. A key tool in making this connection is chiral effective field theory, which organizes the low-energy nuclear interactions of protons and neutrons according to powers of momenta and factors of the pion mass. The most important interactions are included at leading order (LO), the next largest contributions appear at next-to-leading order (NLO), and then next-to-next-to-leading order (NNLO) and so on. See Ref. [16] for a recent review of chiral effective field theory. While the progress in *ab initio* nuclear theory has been impressive, there are gaps in our understanding of the connection between nuclear forces and nuclear structure. In this letter we discover an unexpected twist in the story of how nucleons self-assemble into nuclei. In order to make our calculations transparent and reproducible by others, we remove all non-essential complications from our discussion. For this purpose, we present lattice Monte Carlo simulation results using lattice interactions at LO in chiral effective field theory, together with Coulomb interactions between protons. In the lattice calculations discussed here we use a spatial lattice spacing of 1.97 fm and time lattice spacing of 1.32 fm. We are using natural units where the reduced Planck constant \hbar and the speed of light c equal 1.

Our starting point is two lattice interactions A and B at leading order in chiral effective field theory which are by design similar to each other and tuned to experimental low-energy nucleon-nucleon scattering phase shifts. The details of these interactions and scattering phase shifts are presented in Supplemental Materials at [URL will be inserted by publisher], but we note some important points here. The interactions appear at LO in chiral effective field theory and consist of short-range interactions as well as the potential energy due to the exchange of a pion. As the short-range interactions are not truly point-like, they are actually what we call improved LO interactions. We write the nucleon-nucleon interactions as $V_A(\mathbf{r}', \mathbf{r})$ and $V_B(\mathbf{r}', \mathbf{r})$, where \mathbf{r} is the spatial separation of the two incoming nucleons and \mathbf{r}' is the spatial separation of the two outgoing nucleons. The short-range interactions in $V_A(\mathbf{r}', \mathbf{r})$ consist of nonlocal terms, which means that \mathbf{r}' and \mathbf{r} are in general different. In contrast, the short-range interactions in $V_B(\mathbf{r}', \mathbf{r})$ include nonlocal terms and also local terms where \mathbf{r}' and \mathbf{r} are fixed to be equal. The main difference between interactions A and B is the degree of locality of the short-range interactions. Another difference is that there are extra parameters contained in interaction B, and these are used to reproduce *S*-wave scattering for two alpha particles.

TABLE I: Ground state energies of ^3H , ^3He , ^4He , ^8Be , ^{12}C , ^{16}O , ^{20}Ne for interactions A and B. We show LO results, LO + Coulomb results, and experimental data. All energies are in units of MeV. The error bars denote one standard deviation errors.

Nucleus	A (LO)	B (LO)	A (LO + Coulomb)	B (LO + Coulomb)	Experiment
^3H	-7.82(5)	-7.78(12)	-7.82(5)	-7.78(12)	-8.482
^3He	-7.82(5)	-7.78(12)	-7.08(5)	-7.09(12)	-7.718
^4He	-29.36(4)	-29.19(6)	-28.62(4)	-28.45(6)	-28.296
^8Be	-58.61(14)	-59.73(6)	-56.51(14)	-57.29(7)	-56.591
^{12}C	-88.2(3)	-95.0(5)	-84.0(3)	-89.9(5)	-92.162
^{16}O	-117.5(6)	-135.4(7)	-110.5(6)	-126.0(7)	-127.619
^{20}Ne	-148(1)	-178(1)	-137(1)	-164(1)	-160.645

We have used auxiliary-field Monte Carlo simulations to calculate nuclear ground state energies. In Table I we present the ground state energies of ^3H , ^3He , ^4He , ^8Be , ^{12}C , ^{16}O , ^{20}Ne for interactions A and B. While we use the notation meant for bound nuclei, in some cases the nuclear ground state is an unbound continuum state in our finite periodic box. We do not stabilize against decay to alpha particles. In fact, for the case of interaction A, all of the ground states in Table 1 are multi-alpha states. Details about the size of the box and the initial states used in the Monte Carlo simulations are provided in Supplemental Materials at [URL will be inserted by publisher]. The nuclei ^4He , ^8Be , ^{12}C , ^{16}O , ^{20}Ne are alpha-like nuclei with even and equal numbers of protons and neutrons. We show results at leading order (LO) and leading order with Coulomb interactions between protons (LO + Coulomb), as well as the comparison with experimental data. All energies are in units of MeV. The lattice volume is taken large enough so that the finite-volume energy correction is less than 1% in relative error. The LO + Coulomb results for interaction B are in good agreement with experimental results, better overall than the NNLO results in Ref. [11]. However there is significant underbinding for interaction A with increasing nucleon number. For interaction A, it is illuminating to compute the ratio of the LO energy for each of the alpha-like nuclei to that of the alpha particle. For ^8Be the ratio is 1.997(6), for ^{12}C the ratio is 3.00(1), for ^{16}O it is 4.00(2), and for ^{20}Ne we have 5.03(3). These simple integer ratios indicate that the ground state for interaction A in each case is a weakly-interacting Bose gas of alpha particles. This interpretation is also confirmed by calculations of two-nucleon spatial correlations and local four-nucleon correlations.

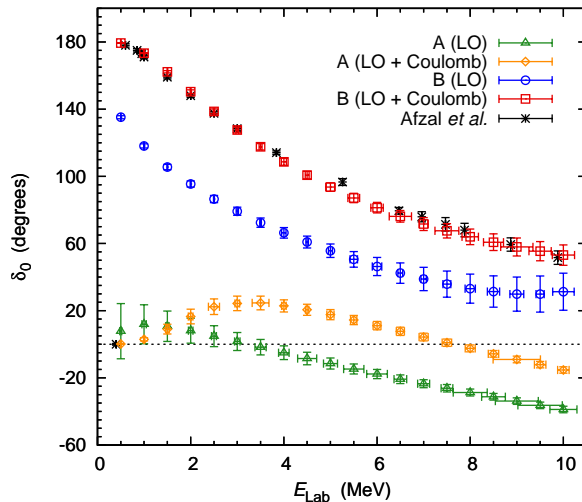
To understand how interactions A and B can produce such completely different physics, we show their alpha-alpha S -wave phase shifts in Fig. 1. The LO results for interaction A are shown with green triangles, LO + Coulomb results for A are orange diamonds, LO results for B are blue circles, and LO + Coulomb results for B are red squares. The experimental data are shown with black asterisks [17]. The phase shifts are computed using auxiliary-field Monte Carlo simulations and a technique called the adiabatic projection method [18]. Interaction B was tuned to the nucleon-nucleon phase shifts and the alpha-alpha S -wave phase shifts, and so the agreement with experimental data is very good. However the phase shifts for interaction A are small and even negative at larger energies. This would explain the large differences between interactions A and B for the energies of the larger alpha-like nuclei in Table I.

What we have discovered is that alpha-alpha scattering is very sensitive to the degree of locality of the nucleon-nucleon lattice interactions. In Supplemental Materials at [URL will be inserted by publisher] we show that this dependence on degree of locality is due to the compactness of the alpha-particle wave function. In contrast, the nucleon-nucleon scattering phase shifts make no constraint on the degree of locality of the nucleon-nucleon interactions. For example, if one starts with a purely local interaction, a unitary transformation can be used to define a new interaction which is highly nonlocal but having exactly the same phase shifts. The differences only become apparent in systems with more than two nucleons and can be understood as arising from three-body and higher-body interactions [19, 20]. Interaction A is a perfectly valid starting point for describing nucleon-nucleon interactions. However, substantial higher-nucleon interactions will be needed to rectify the missing strength of the alpha-alpha interactions and the additional binding energy in nuclei.

The results we have found here suggests a strategy for improving future *ab initio* nuclear structure and reaction calculations by incorporating low-energy light-nucleus scattering data in addition to nucleon-nucleon scattering data. This would be especially important for accurate calculations of key alpha capture reactions relevant to astrophysics such as alpha capture on ^{12}C [21]. One can view the extra step of fixing the degree of locality of the nucleon-nucleon interaction as preemptively reducing the importance of the required three-body and higher-body interactions. It is similar in spirit to other approaches that use nuclear structure and many-body observables to help determine the nucleon-nucleon interactions [15, 22, 23].

Since alpha-alpha scattering is a difficult and computationally-intensive *ab initio* calculation, it is useful to discuss a simple qualitative picture of the alpha-alpha interaction in a tight-binding approximation. For any nucleon-nucleon

FIG. 1: Alpha-alpha S -wave scattering. We plot S -wave phase shifts δ_0 for alpha-alpha scattering for interactions A and B versus laboratory energy. We show LO results for interaction A (green triangles), LO + Coulomb for A (orange diamonds), LO results for B (blue circles), and LO + Coulomb results for B (red squares). The phase shift analysis of experimental data are shown with black asterisks [17]. The theoretical error bars indicate one standard deviation uncertainty due to Monte Carlo errors and the extrapolation to infinite number of time steps.



interaction $V(\mathbf{r}', \mathbf{r})$, we define the tight-binding potential, $V_{\text{TB}}(r)$, as the contribution that $V(\mathbf{r}', \mathbf{r})$ makes to the effective interaction between alpha particles in the tight-binding approximation where the alpha particle radius R_α is treated as a small but non-vanishing length scale. In this simple approximation the interaction $V(\mathbf{r}', \mathbf{r})$ contributes to the effective alpha-alpha interaction only in two possible ways. The first is what we call the direct term where $|\mathbf{r}' - \mathbf{r}| \lesssim R_\alpha$, and the second is the exchange term where $|\mathbf{r}' + \mathbf{r}| \lesssim R_\alpha$. All other terms are forbidden because the interaction is moving the nucleons to locations where there are no alpha particles. For the LO lattice interactions we consider here at lattice spacing 1.97 fm, we do not attempt to resolve the different microscopic mechanisms that can contribute to $V_{\text{TB}}(r)$. However calculations at smaller lattice spacings would find that the two-pion exchange interaction is responsible for a large attractive tight-binding potential at NNLO [16]. This observation connects well with the work of Ref. [24], which considered the role of the two-pion exchange interaction in an effective field theory where alpha particles are treated as fundamental objects.

In Fig. 2 we show the tight-binding potential for the LO lattice interactions for A and B. For our lattice calculations where space is discrete, we find that R_α is less than one lattice spacing and so the dependence on R_α drops out. We see that interaction A has a very small tight-binding potential. This is consistent with the weak alpha-alpha S -wave interactions found in Fig. 1. In contrast, interaction B has a stronger attractive tight-binding potential resulting from its short-range spin-isospin-independent local interaction. For comparison we also show in Fig. 2 the tight-binding potential for the leading-order interaction used in prior lattice calculations, which we call interaction C [11, 18].

In order to discuss the many-body limit, we switch off the Coulomb interactions and define a one-parameter family of interactions, $V_\lambda = (1 - \lambda)V_A + \lambda V_B$. While the properties of the two, three, and four nucleon systems vary only slightly with λ , the many-body ground state of V_λ undergoes a quantum phase transition from a Bose-condensed gas to a nuclear liquid.

We sketch the zero temperature phase diagram in Fig. 3. The phase transition occurs when the alpha-alpha S -wave scattering length $a_{\alpha\alpha}$ crosses zero, and the Bose gas collapses due to the attractive interactions [25, 26]. At slightly larger λ , finite alpha-like nuclei also become bound, starting with the largest nuclei first. The last alpha-like nucleus to be bound is ${}^8\text{Be}$ at the so-called unitarity point where $|a_{\alpha\alpha}| = \infty$. Superimposed on the phase diagram, we have sketched the alpha-like nuclear ground state energies E_A for A nucleons up to $A = 20$ relative to the corresponding multi-alpha threshold $E_\alpha A/4$. Empirically we find that the quantum phase transition occurs at the point $\lambda_\infty = 0.0(1)$. The uncertainty of ± 0.1 is due to the energy levels having a slow dependence on λ near $\lambda = 0.0$. Since any V_λ represents a seemingly reasonable starting point for the effective field theory at LO, one may end up crossing the phase transition when considering higher-order effects beyond LO. It is in this sense that we say nature is near a quantum phase transition.

The critical point for the binding of ${}^{20}\text{Ne}$ occurs at $\lambda_{20} = 0.2(1)$. For the binding of the other alpha nuclei, we obtain

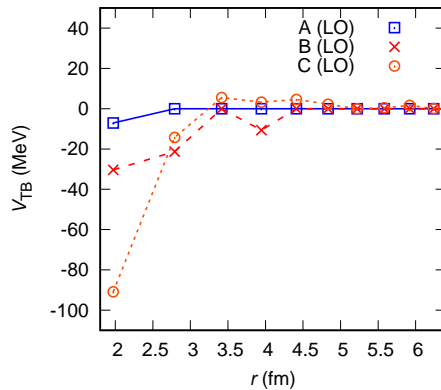
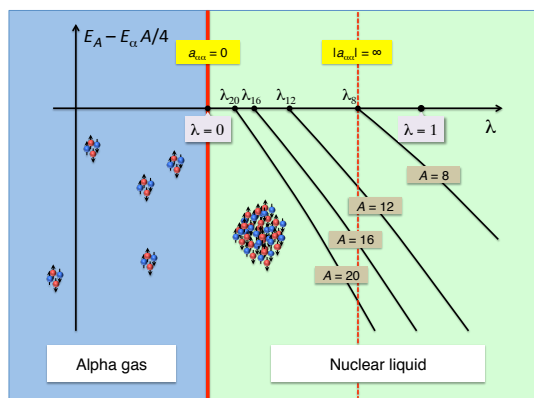


FIG. 2: Tight-binding potential. We plot the tight-binding potential versus radial distance for the LO interactions for A, B, and C, where C is the interaction used in several previous lattice calculations [11, 18]. Interaction A is shown with blue squares and solid line, B is drawn with red crosses and dashed line, and C is presented with orange circles and short-dashed line.

$\lambda_{16} = 0.2(1)$ for ^{16}O , $\lambda_{12} = 0.3(1)$ for ^{12}C , and $\lambda_8 = 0.7(1)$ for ^8Be . One finds a sudden change in the nucleon-nucleon density correlations at long distances as λ crosses the critical point, going from a continuum state to a self-bound system. As λ increases further beyond this critical value, the nucleus becomes more tightly bound, gradually losing its alpha cluster substructure and becoming more like a nuclear liquid droplet. The quantum phase transition at $\lambda_\infty = 0.0(1)$ is the corresponding phenomenon in the many-body system, a first-order phase transition occurring for infinite matter.

FIG. 3: Zero-temperature phase diagram. We show the zero-temperature phase diagram as a function of the parameter λ in the interaction $V_\lambda = (1 - \lambda)V_A + \lambda V_B$ without Coulomb included. The blue filled circles indicate neutrons, the red filled circles indicate protons, and the small arrows attached to the circles indicate spin direction. We show a first-order quantum phase transition from a Bose gas to nuclear liquid at the point where the scattering length $a_{\alpha\alpha}$ crosses zero. We have also plotted the alpha-like nuclear ground state energies E_A for A nucleons up to $A = 20$ relative to the corresponding multi-alpha threshold $E_\alpha A/4$. The last alpha-like nucleus to be bound is ^8Be at the unitarity point where $|a_{\alpha\alpha}| = \infty$.



By adjusting λ in *ab initio* calculations, we have a new tool for studying alpha cluster states such as the Hoyle state of ^{12}C and possible rotational excitations of the Hoyle state [1–6]. By tuning λ to the unitarity point $|a_{\alpha\alpha}| = \infty$, we can continuously connect the Hoyle state wave function without Coulomb interactions to a universal Efimov trimer [7, 8, 27]. An Efimov trimer is one of an infinite tower of three-body states for bosons in the large scattering-length limit, with intriguing mathematical properties such as fractal-like discrete scale invariance. Another interesting system is the second 0^+ state of ^{16}O [28], which should be continuously connected to a universal Efimov tetramer [27, 29, 30]. This connection to Efimov states is now being investigated in follow-up work. The ability to tune the energies of alpha cluster states relative to alpha-separation thresholds provides a new window on wave functions and rotational excitations of alpha cluster states. By studying the λ -dependence of nuclear energy levels one can also identify the

underlying cluster substructure. For example, the energy of a nuclear state which is a weakly-bound collection of four alpha clusters will track closely with the four-alpha threshold $4E_{4\text{He}}$ as a function of λ , while a state which is comprised of ^{12}C and ^4He clusters will track more closely with $E_{^{12}\text{C}} + E_{^4\text{He}}$. Such an analysis may provide a new theoretical foundation for understanding clustering in nuclei and complement existing work on clustering in the literature [31–36], thereby strengthening the theoretical motivation for experimental searches of alpha cluster states in alpha-like nuclei.

Acknowledgement

We acknowledge discussions with Hans-Werner Hammer, Thomas Luu, Lucas Platter, and Thomas Schäfer and partial financial support from the Deutsche Forschungsgemeinschaft (Sino-German CRC 110), the Helmholtz Association (Contract No. VH-VI-417), BMBF (Grant No. 05P12PDFTE), the U.S. Department of Energy (DE-FG02-03ER41260), and U.S. National Science Foundation grant No. PHY-1307453. Further support was provided by the EU HadronPhysics3 project, the ERC Project No. 259218 NUCLEAREFT, the Magnus Ehrnrooth Foundation of the Finnish Society of Sciences and Letters, MINECO (Spain), the ERDF (European Commission) grant FPA2013-40483-P, and the Chinese Academy of Sciences (CAS) President’s International Fellowship Initiative (PIFI) grant no. 2015VMA076. The computational resources were provided by the Jülich Supercomputing Centre at Forschungszentrum Jülich and by RWTH Aachen.

Supplemental Materials

Lattice interactions

For our LO lattice calculations we use a spatial lattice spacing $a = (100 \text{ MeV})^{-1} = 1.97 \text{ fm}$ and time lattice step $a_t = (150 \text{ MeV})^{-1} = 1.32 \text{ fm}$. Our axial-vector coupling constant is $g_A = 1.29$ as derived from the Goldberger-Treiman relation, the pion decay constant is $f_\pi = 92.2 \text{ MeV}$, and the pion mass is $M_\pi = M_{\pi^0} = 134.98 \text{ MeV}$. For the nucleon mass we use $m = 938.92 \text{ MeV}$, and the electromagnetic fine structure constant is $\alpha_{\text{EM}} = (137.04)^{-1}$. We don't consider any isospin-breaking terms other than the Coulomb interaction in these LO calculations. We use σ_S with $S = 1, 2, 3$ for the Pauli matrices acting upon spin, and τ_I with $I = 1, 2, 3$ for the Pauli matrices acting upon isospin. We will use lattice units where the quantities are multiplied by the appropriate power of the spatial lattice spacing a to make the combination dimensionless. We write α_t for the ratio a_t/a . We use the notation $\sum_{\langle \mathbf{n}' \mathbf{n} \rangle}$ to denote the summation over nearest-neighbor lattice sites of \mathbf{n} . We write $\sum_{\langle \mathbf{n}' \mathbf{n} \rangle_i}$ to indicate the sum over nearest-neighbor lattice sites of \mathbf{n} along the i^{th} spatial axis. Similarly, we define $\sum_{\langle\langle \mathbf{n}' \mathbf{n} \rangle\rangle_i}$ as the sum over next-to-nearest-neighbor lattice sites of \mathbf{n} along the i^{th} axis and $\sum_{\langle\langle\langle \mathbf{n}' \mathbf{n} \rangle\rangle\rangle_i}$ as the sum over next-to-next-to-nearest-neighbor lattice sites of \mathbf{n} along the i^{th} axis. Our lattice geometry is chosen to be an L^3 periodic lattice, and so the summations over \mathbf{n}' are defined using periodic boundary conditions.

For each lattice site \mathbf{n} on our lattice and real parameter s_{NL} , we define nonlocal annihilation and creation operators for each spin and isospin component of the nucleon,

$$a_{\text{NL}}(\mathbf{n}) = a(\mathbf{n}) + s_{\text{NL}} \sum_{\langle \mathbf{n}' \mathbf{n} \rangle} a(\mathbf{n}'), \quad (1)$$

$$a_{\text{NL}}^\dagger(\mathbf{n}) = a^\dagger(\mathbf{n}) + s_{\text{NL}} \sum_{\langle \mathbf{n}' \mathbf{n} \rangle} a^\dagger(\mathbf{n}'). \quad (2)$$

For spin indices $S = 1, 2, 3$, and isospin indices $I = 1, 2, 3$, we define point-like densities,

$$\rho(\mathbf{n}) = a^\dagger(\mathbf{n})a(\mathbf{n}), \quad (3)$$

$$\rho_S(\mathbf{n}) = a^\dagger(\mathbf{n})[\sigma_S]a(\mathbf{n}), \quad (4)$$

$$\rho_I(\mathbf{n}) = a^\dagger(\mathbf{n})[\tau_I]a(\mathbf{n}), \quad (5)$$

$$\rho_{S,I}(\mathbf{n}) = a^\dagger(\mathbf{n})[\sigma_S \otimes \tau_I]a(\mathbf{n}). \quad (6)$$

For spin indices $S = 1, 2, 3$, and isospin indices $I = 1, 2, 3$, we also define smeared nonlocal densities,

$$\rho_{\text{NL}}(\mathbf{n}) = a_{\text{NL}}^\dagger(\mathbf{n})a_{\text{NL}}(\mathbf{n}), \quad (7)$$

$$\rho_{S,\text{NL}}(\mathbf{n}) = a_{\text{NL}}^\dagger(\mathbf{n})[\sigma_S]a_{\text{NL}}(\mathbf{n}), \quad (8)$$

$$\rho_{I,\text{NL}}(\mathbf{n}) = a_{\text{NL}}^\dagger(\mathbf{n})[\tau_I]a_{\text{NL}}(\mathbf{n}), \quad (9)$$

$$\rho_{S,I,\text{NL}}(\mathbf{n}) = a_{\text{NL}}^\dagger(\mathbf{n})[\sigma_S \otimes \tau_I]a_{\text{NL}}(\mathbf{n}), \quad (10)$$

and smeared local densities for real parameter s_L ,

$$\rho_L(\mathbf{n}) = a^\dagger(\mathbf{n})a(\mathbf{n}) + s_L \sum_{\langle \mathbf{n}' \mathbf{n} \rangle} a^\dagger(\mathbf{n}')a(\mathbf{n}'), \quad (11)$$

$$\rho_{S,L}(\mathbf{n}) = a^\dagger(\mathbf{n})[\sigma_S]a(\mathbf{n}) + s_L \sum_{\langle \mathbf{n}' \mathbf{n} \rangle} a^\dagger(\mathbf{n}')[\sigma_S]a(\mathbf{n}'), \quad (12)$$

$$\rho_{I,L}(\mathbf{n}) = a^\dagger(\mathbf{n})[\tau_I]a(\mathbf{n}) + s_L \sum_{\langle \mathbf{n}' \mathbf{n} \rangle} a^\dagger(\mathbf{n}')[\tau_I]a(\mathbf{n}'), \quad (13)$$

$$\rho_{S,I,L}(\mathbf{n}) = a^\dagger(\mathbf{n})[\sigma_S \otimes \tau_I]a(\mathbf{n}) + s_L \sum_{\langle \mathbf{n}' \mathbf{n} \rangle} a^\dagger(\mathbf{n}')[\sigma_S \otimes \tau_I]a(\mathbf{n}'). \quad (14)$$

The nonlocal short-range interactions are written as

$$V_{\text{NL}} = \frac{c_{\text{NL}}}{2} \sum_{\mathbf{n}} : \rho_{\text{NL}}(\mathbf{n})\rho_{\text{NL}}(\mathbf{n}) : + \frac{c_{I,\text{NL}}}{2} \sum_{\mathbf{n},I} : \rho_{I,\text{NL}}(\mathbf{n})\rho_{I,\text{NL}}(\mathbf{n}) :, \quad (15)$$

while the local short-range interactions are

$$V_L = \frac{c_L}{2} \sum_{\mathbf{n}} : \rho_L(\mathbf{n}) \rho_L(\mathbf{n}) : + \frac{c_{S,L}}{2} \sum_{\mathbf{n},S} : \rho_{S,L}(\mathbf{n}) \rho_{S,L}(\mathbf{n}) : \\ + \frac{c_{I,L}}{2} \sum_{\mathbf{n},I} : \rho_{I,L}(\mathbf{n}) \rho_{I,L}(\mathbf{n}) : + \frac{c_{S,I,L}}{2} \sum_{\mathbf{n},S,I} : \rho_{S,I,L}(\mathbf{n}) \rho_{S,I,L}(\mathbf{n}) : . \quad (16)$$

The $::$ symbol indicates normal ordering, where the annihilation operators are on the right-hand side and the creation operators are on the left-hand side. As described in previous work [37], we take special combinations of the four local short-range operator coefficients so that the interaction in odd partial waves vanish completely. For our work here, we also make the strength of the local short-range interactions equal in the two S -wave channels. As a result, we have only one independent coefficient, $c_{S,L} = c_{I,L} = c_{S,I,L} = -\frac{1}{3}c_L$. In future work it may be useful to consider relaxing this condition.

The one-pion exchange interaction has the form

$$V_{\text{OPE}} = -\frac{g_A^2}{8f_\pi^2} \sum_{\mathbf{n}',\mathbf{n},S',S,I} : \rho_{S',I}(\mathbf{n}') f_{S'S}(\mathbf{n}' - \mathbf{n}) \rho_{S,I}(\mathbf{n}) :, \quad (17)$$

where $f_{S'S}$ is defined as

$$f_{S'S}(\mathbf{n}' - \mathbf{n}) = \frac{1}{L^3} \sum_{\mathbf{q}} \frac{\exp[-i\mathbf{q} \cdot (\mathbf{n}' - \mathbf{n}) - b_\pi \mathbf{q}^2] q_{S'} q_S}{\mathbf{q}^2 + M_\pi^2}, \quad (18)$$

and each lattice momentum component q_S is an integer multiplied by $2\pi/L$. The parameter b_π is included to remove short-distance lattice artifacts in the one-pion exchange interaction. It results in better preservation of rotational symmetry and will be especially useful at smaller lattice spacings [38]. The Coulomb interaction can be written as

$$V_{\text{Coulomb}} = -\frac{\alpha_{\text{EM}}}{2} \sum_{\mathbf{n}',\mathbf{n}} : \frac{1}{4} [\rho(\mathbf{n}') + \rho_{I=3}(\mathbf{n}')] \frac{1}{d(\mathbf{n}' - \mathbf{n})} [\rho(\mathbf{n}) + \rho_{I=3}(\mathbf{n})] :, \quad (19)$$

where $d(\mathbf{n}' - \mathbf{n})$ is the shortest length of $\mathbf{n}' - \mathbf{n}$ as measured on the periodic lattice, and we define the value of d at the origin to be $\frac{1}{2}$. Our notation $\rho_{I=3}$ refers to the $I = 3$ isospin component of ρ_I . We use a free lattice Hamiltonian [37] of the form,

$$H_{\text{free}} = \frac{49}{12m} \sum_{\mathbf{n}} a^\dagger(\mathbf{n}) a(\mathbf{n}) - \frac{3}{4m} \sum_{\mathbf{n},i} \sum_{\langle \mathbf{n}' \mathbf{n} \rangle_i} a^\dagger(\mathbf{n}') a(\mathbf{n}) \\ + \frac{3}{40m} \sum_{\mathbf{n},i} \sum_{\langle\langle \mathbf{n}' \mathbf{n} \rangle\rangle_i} a^\dagger(\mathbf{n}') a(\mathbf{n}) - \frac{1}{180m} \sum_{\mathbf{n},i} \sum_{\langle\langle\langle \mathbf{n}' \mathbf{n} \rangle\rangle\rangle_i} a^\dagger(\mathbf{n}') a(\mathbf{n}). \quad (20)$$

For interaction A at LO, the lattice Hamiltonian is

$$H_A = H_{\text{free}} + V_{\text{NL}} + V_{\text{OPE}}, \quad (21)$$

with $s_{\text{NL}} = 0.07700$, $c_{\text{NL}} = -0.2268$, $c_{I,\text{NL}} = 0.02184$, and $b_\pi = 0.7000$. These parameters are determined by fitting to the low-energy nucleon-nucleon phase shifts and the observed deuteron energy. For the corresponding LO + Coulomb interactions, we simply add V_{Coulomb} to H_A .

For interaction B at LO, we have

$$H_B = H_{\text{free}} + V_{\text{NL}} + V_L + V_{\text{OPE}}, \quad (22)$$

with $s_{\text{NL}} = 0.07700$, $s_L = 0.8100$, $c_{\text{NL}} = -0.1171$, $c_{I,\text{NL}} = 0.02607$, $c_L = -0.01013$, and $b_\pi = 0.7000$. For the corresponding LO + Coulomb interactions, we simply add V_{Coulomb} to H_B . These parameters are determined by fitting to the low-energy nucleon-nucleon phase shifts, the observed deuteron energy, and the low-energy alpha-alpha S -wave phase shifts.

We should clarify that the ${}^4\text{He}$ energy is not used to fit the parameters of interactions A and B. However we do observe a strong correlation between the alpha-alpha S -wave phase shifts and the shape of the ${}^4\text{He}$ wave function tail. This has the resulting effect of driving the ${}^4\text{He}$ energy close to the physical value when we tune the parameters of interaction B to the alpha-alpha S -wave phase shifts. The parameters of interaction A are determined by starting from the parameters of interaction B, setting the local short-range interactions to zero, and then tuning the coefficients of the nonlocal short-range interactions to the nucleon-nucleon phase shifts and deuteron energy.

Nucleon-nucleon scattering

We use the spherical wall method to calculate lattice phase shifts [39, 40]. We use the improvements recently introduced in Ref. [41]. Let $|\mathbf{n}\rangle \otimes |S_z\rangle$ be the two-nucleon scattering state with lattice separation vector \mathbf{n} and z -component of total intrinsic spin S_z . We define radial coordinates on the lattice by grouping together lattice mesh points with the same radial distance to define radial position states and project onto states with total angular momentum J, J_z in the continuum limit. Using spherical harmonics Y_{ℓ, ℓ_z} with orbital angular momentum ℓ, ℓ_z and Clebsch-Gordan coefficients $C_{\ell, \ell_z, S, S_z}^{J, J_z}$, we define

$$|r\rangle_L^{J, J_z} = \sum_{\mathbf{n}, \ell_z, S_z} C_{\ell, \ell_z, S, S_z}^{J, J_z} Y_{\ell, \ell_z}(\hat{\mathbf{n}}) \delta_{r, |\mathbf{n}|} |\mathbf{n}\rangle \otimes |S_z\rangle, \quad (23)$$

where $\delta_{r, |\mathbf{n}|}$ is a Kronecker delta function that selects lattice points where $|\mathbf{n}| = r$. This angular momentum projection allows us to calculate partial-wave phase shifts on the lattice as in Ref. [41].

As described in Ref. [41], we impose a hard spherical wall boundary at some large radius R_W and a smooth auxiliary Gaussian potential in front of the wall, which we call $V_{\text{aux}}(r)$. For our calculations here we use $R_W = 15.02$ lattice units. The auxiliary potential has the form

$$V_{\text{aux}}(r) = V_0 \exp[-(r - R_W)^2], \quad (24)$$

with adjustable coefficient V_0 that is used to probe different values of the scattering energy. The auxiliary potential is non-negligible only when r is a few lattice units away the wall at R_W . We determine the asymptotic phase shifts from the radial wave function at points where r is large but $V_{\text{aux}}(r)$ is negligible. For coupled partial waves such as the ${}^3s_1 - {}^3d_1$ channel, we determine the two phase shifts and mixing angle using an additional auxiliary potential $U_{\text{aux}}(r)$ with the same functional form as $V_{\text{aux}}(r)$, but with imaginary Hermitian off-diagonal couplings between the two partial waves,

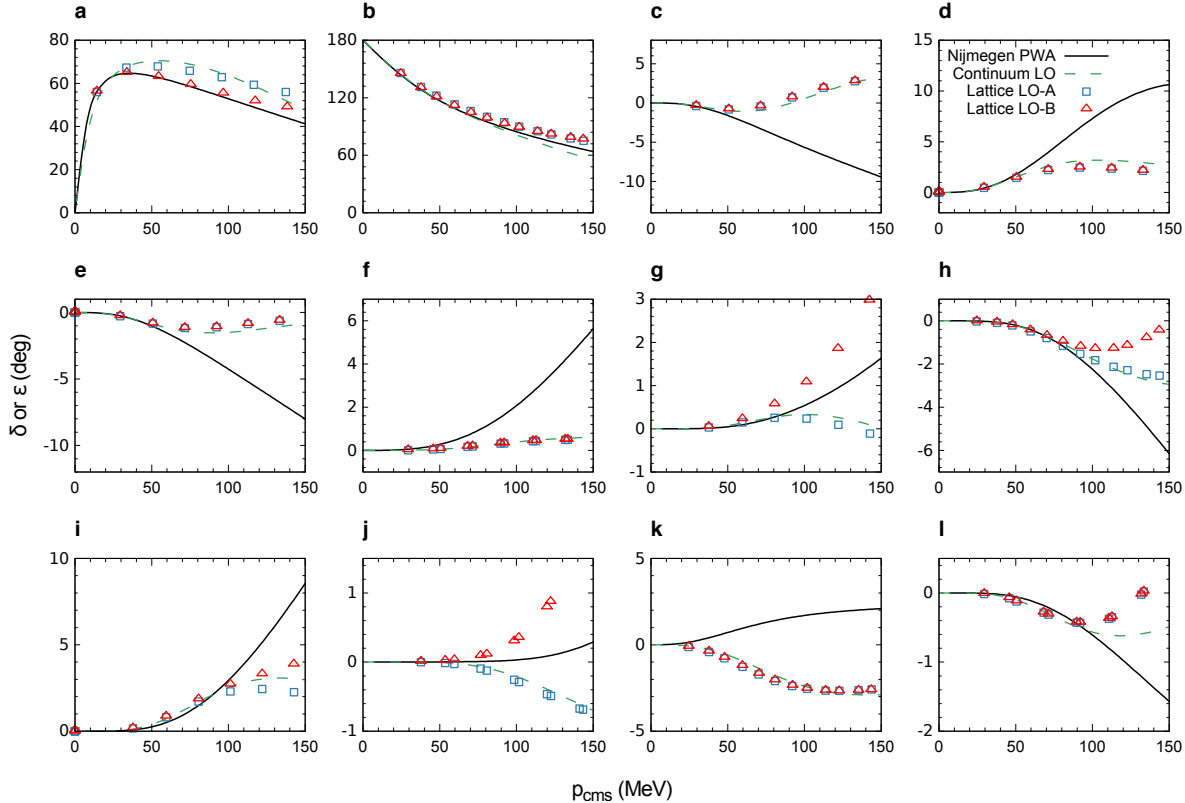
$$\begin{bmatrix} 0 & iU_{\text{aux}}(r) \\ -iU_{\text{aux}}(r) & 0 \end{bmatrix}. \quad (25)$$

This complex-valued auxiliary potential breaks time-reversal invariance and allows us to extract information about the two independent phase shifts and mixing angle from the real and imaginary parts of the complex-valued wave functions.

In Fig. 4 we show LO lattice phase shifts for proton-neutron scattering versus the center-of-mass relative momentum for interactions A (red triangles) and B (blue squares). For comparison we also plot the phase shifts extracted from the Nijmegen partial wave analysis [42] (black lines) and a continuum version of interaction A (green dashed lines). In the first row, the data in panels **a**, **b**, **c**, **d** correspond to ${}^1S_0, {}^3S_1, {}^1P_1, {}^3P_0$ respectively. In the second row, panels **e**, **f**, **g**, **h** correspond to ${}^3P_1, {}^3P_2, {}^1D_2, {}^3D_1$ respectively. In the third row, panels **i**, **j**, **k**, **l** correspond to ${}^3D_2, {}^3D_3, \varepsilon_1, \varepsilon_2$ respectively. The level of agreement with the experimental phase shifts for interactions A and B is typical for LO chiral effective field theory at our cutoff momentum of $\pi/a \approx 314$ MeV. The agreement would be somewhat better if we were to use a smaller value of the smearing parameter b_π in the one-pion exchange potential. However, we prefer the higher value of b_π to reduce sign oscillations in the Monte Carlo lattice simulations. The LO interactions are more than sufficient to illustrate the ideas of this work but not sufficient for precision calculations. For precision calculations, this would be just the first step in the chiral effective field theory expansion, and the phase shifts would be systematically improved at each higher order, NLO, NNLO, and so on.

We note the good agreement between the continuum results in green dashed lines and lattice interaction A results. This is a good indication that we have successfully reduced lattice artifacts from the calculations and was part of the motivation for introducing the parameter b_π . The nonlocal smeared interaction V_{NL} makes a non-negligible contribution to the S -wave interactions only. Furthermore, the local smeared interaction V_{L} makes a nonzero contribution to only the even partial waves (S, D, \dots). Hence the interactions A and B are exactly the same in all odd partial waves. We see that the S -wave interactions for interactions A and B are also quite similar, though the 1S_0 partial wave scattering is somewhat more attractive for interaction A. On the other hand, the D -wave partial waves are more attractive for interaction B.

FIG. 4: Nucleon-nucleon scattering phase shifts. We plot LO lattice phase shifts for proton-neutron scattering versus the center-of-mass relative momentum for interactions A (red triangles) and B (blue squares). For comparison we also plot the phase shifts extracted from the Nijmegen partial wave analysis [42] (black lines) and a continuum version of interaction A (green dashed lines). In the first row, the data in panels **a**, **b**, **c**, **d** correspond to 1S_0 , 3S_1 , 1P_1 , 3P_0 respectively. In the second row, panels **e**, **f**, **g**, **h** correspond to 3P_1 , 3P_2 , 1D_2 , 3D_1 respectively. In the third row, panels **i**, **j**, **k**, **l** correspond to 3D_2 , 3D_3 , ε_1 , ε_2 respectively.



Euclidean time projection and auxiliary-field Monte Carlo

In these lattice simulations we work with the Euclidean time transfer matrix M , which is defined as the normal-ordered exponential of the lattice Hamiltonian H over one time lattice step,

$$M =: \exp[-H\alpha_t] : . \quad (26)$$

We consider some initial state $|\Psi_i\rangle$ and final state $|\Psi_f\rangle$ that have nonzero overlap with the ground state of interest. By applying successive powers of M upon $|\Psi_i\rangle$, the excited states decay away, and we can project out only the ground state. We calculate projection amplitudes of the form

$$A_{fi}(L_t) = \langle \Psi_f | M^{L_t} | \Psi_i \rangle. \quad (27)$$

By calculating the ratio $A_{fi}(L_t)/A_{fi}(L_t - 1)$ for large L_t we can determine the ground state energy. In order to calculate first-order corrections to the ground state energy due to an additional term ΔH in the Hamiltonian, we also calculate the projection amplitude

$$A_{fi}^\Delta(L_t) = \langle \Psi_f | M^{\frac{L_t-1}{2}} M_\Delta M^{\frac{L_t-1}{2}} | \Psi_i \rangle, \quad (28)$$

for odd L_t , where

$$M_\Delta =: \exp[-(H + \Delta H)\alpha_t] : . \quad (29)$$

The corrections due to H_{Coulomb} are computed in this manner.

In most cases it is advantageous to first prepare the initial state using a simpler transfer matrix M_* which is an approximation to M . We choose M_* to be invariant under Wigner's SU(4) symmetry [43] where the four spin-isospin combinations of the nucleon transform into one another. The SU(4) symmetry eliminates sign oscillations from auxiliary-field Monte Carlo simulations of M_* [44, 45]. M_* has the same form as M , but the coefficients of operators that violate SU(4) symmetry are turned off. We use M_* as an approximate low-energy filter by multiplying the initial and final states by M_* for some fixed number of times, L'_t ,

$$A_{fi}(L_t) = \langle \Psi_f | M_*^{L'_t} M^{L_t} M_*^{L'_t} | \Psi_i \rangle. \quad (30)$$

We use auxiliary fields to generate the interactions contained in our lattice Hamiltonian. The auxiliary field method can be understood as a Gaussian integral formula which relates the exponential of the two-particle density, ρ^2 , to the integral of the exponential of the one-particle density, ρ ,

$$: \exp\left(-\frac{c\alpha_t}{2}\rho^2\right) : = \sqrt{\frac{1}{2\pi}} \int_{-\infty}^{\infty} ds : \exp\left(-\frac{1}{2}s^2 + \sqrt{-c\alpha_t}s\rho\right) :. \quad (31)$$

The normal ordering symbol $::$ ensures that the operator products of the creation and annihilation operators are treated as though classical anticommuting Grassmann variables [46]. We use this integral identity to introduce auxiliary fields defined over every lattice point in space and time [47–49]. As we will see shortly, the pion fields are treated in a manner similar to the auxiliary fields. Each nucleon is independent of the other nucleons and interacts only with the auxiliary and pion fields. If the initial and final states are an antisymmetric tensor product of A single nucleon states, then the projection amplitude for any configuration of auxiliary and pion fields is proportional to the determinant of an $A \times A$ matrix Z_{jk} . The matrix entries of Z_{jk} are single nucleon amplitudes for a nucleon starting at state k and ending at state j .

We couple auxiliary fields s to ρ_{NL} and s_I to $\rho_{I,\text{NL}}$ for the nonlocal interactions in V_{NL} . The terms linear in the auxiliary fields are

$$V_{\text{NL}}^s = \sqrt{-c_{\text{NL}}} \sum_{\mathbf{n}} \rho_{\text{NL}}(\mathbf{n}) s(\mathbf{n}) + \sqrt{-c_{I,\text{NL}}} \sum_{\mathbf{n},I} \rho_{I,\text{NL}}(\mathbf{n}) s_I(\mathbf{n}), \quad (32)$$

and the terms quadratic field in the auxiliary fields are

$$V_{\text{NL}}^{ss} = \frac{1}{2} \sum_{\mathbf{n}} s^2(\mathbf{n}) + \frac{1}{2} \sum_{\mathbf{n},I} s_I^2(\mathbf{n}). \quad (33)$$

We also couple auxiliary fields u to ρ_L , u_S to $\rho_{S,L}$, u_I to $\rho_{I,L}$, and $u_{S,I}$ to $\rho_{S,I,L}$, for the local interactions in V_L ,

$$\begin{aligned} V_L^u &= \sqrt{-c_L} \sum_{\mathbf{n}} \rho_L(\mathbf{n}) u(\mathbf{n}) + \sqrt{-c_{S,L}} \sum_{\mathbf{n},S} \rho_{S,L}(\mathbf{n}) u_S(\mathbf{n}) \\ &+ \sqrt{-c_{I,L}} \sum_{\mathbf{n},I} \rho_{I,L}(\mathbf{n}) u_I(\mathbf{n}) + \sqrt{-c_{S,I,L}} \sum_{\mathbf{n},S,I} \rho_{S,I,L}(\mathbf{n}) u_{S,I}(\mathbf{n}), \end{aligned} \quad (34)$$

$$V_L^{uu} = \frac{1}{2} \sum_{\mathbf{n}} u^2(\mathbf{n}) + \frac{1}{2} \sum_{\mathbf{n},S} u_S^2(\mathbf{n}) + \frac{1}{2} \sum_{\mathbf{n},I} u_I^2(\mathbf{n}) + \frac{1}{2} \sum_{\mathbf{n},S,I} u_{S,I}^2(\mathbf{n}). \quad (35)$$

For the one-pion exchange interaction we couple the gradient of the pion field π_I to the point-like density $\rho_{S,I}$,

$$V^\pi = \frac{g_A}{2f_\pi} \sum_{\mathbf{n},S,I} \rho_{S,I}(\mathbf{n}') f_S^\pi(\mathbf{n}' - \mathbf{n}) \pi_I(\mathbf{n}), \quad (36)$$

$$V^{\pi\pi} = \frac{1}{2} \sum_{\mathbf{n},I} \pi_I(\mathbf{n}') f^{\pi\pi}(\mathbf{n}' - \mathbf{n}) \pi_I(\mathbf{n}) :, \quad (37)$$

where f_S^π and $f^{\pi\pi}$ are defined as

$$f_S^\pi(\mathbf{n}' - \mathbf{n}) = \frac{1}{L^3} \sum_{\mathbf{q}} \exp[-i\mathbf{q} \cdot (\mathbf{n}' - \mathbf{n})] q_S, \quad (38)$$

$$f^{\pi\pi}(\mathbf{n}'-\mathbf{n}) = \frac{1}{L^3} \sum_{\mathbf{q}} \exp[-i\mathbf{q} \cdot (\mathbf{n}' - \mathbf{n}) + b_{\pi}\mathbf{q}^2](\mathbf{q}^2 + m_{\pi}^2). \quad (39)$$

Then the transfer matrices for the LO interactions can be written in following manner. For interaction A we have

$$: \exp(-H_A \alpha_t) := \int Ds D\pi : \exp(-H_{\text{free}} \alpha_t - V_{\text{NL}}^s \sqrt{\alpha_t} - V_{\text{NL}}^{ss} - V^{\pi} \alpha_t - V^{\pi\pi} \alpha_t) :, \quad (40)$$

where Ds is the path integral measure for s and s_I , and $D\pi$ is the path integral measure for π_I . For interaction B we find

$$: \exp(-H_B \alpha_t) := \int Du Du D\pi : \exp(-H_{\text{free}} \alpha_t - V_{\text{NL}}^s \sqrt{\alpha_t} - V_{\text{NL}}^{ss} - V_L^u \sqrt{\alpha_t} - V_L^{uu} - V^{\pi} \alpha_t - V^{\pi\pi} \alpha_t) :, \quad (41)$$

where Du is the path integral measure for u , u_S , u_I , and $u_{S,I}$. See Ref. [46] for details on the Monte Carlo importance sampling algorithms used to calculate the path integrals over the auxiliary and pion fields.

When computing the energy from ratios of amplitudes $A_{fi}(L_t)/A_{fi}(L_t-1)$, previous studies have used importance sampling according to the importance function $|A_{fi}(L_t-1)|$ or $|A_{fi}(L_t)|$. In this work we sample according to a linear combination $x|A_{fi}(L_t-1)| + (1-x)|A_{fi}(L_t)|$ where $0 < x < 1$. This greatly reduces the stochastic noise because the contributions to $A_{fi}(L_t-1)$ and $A_{fi}(L_t)$ from any individual configuration are now bounded above in magnitude,

$$\frac{|A_{fi}(L_t-1)|}{x|A_{fi}(L_t-1)| + (1-x)|A_{fi}(L_t)|} < x^{-1}, \quad (42)$$

$$\frac{|A_{fi}(L_t)|}{x|A_{fi}(L_t-1)| + (1-x)|A_{fi}(L_t)|} < (1-x)^{-1}. \quad (43)$$

Ground state energies of nuclei

We let $a_{\uparrow,p}^{\dagger}(\mathbf{n})$, $a_{\downarrow,p}^{\dagger}(\mathbf{n})$, $a_{\uparrow,n}^{\dagger}(\mathbf{n})$, and $a_{\downarrow,n}^{\dagger}(\mathbf{n})$ be the creation operators for a spin-up proton, spin-down proton, spin-up neutron, and spin-down neutron. We write $\tilde{a}_{\uparrow,p}^{\dagger}(0)$, $\tilde{a}_{\downarrow,p}^{\dagger}(0)$, $\tilde{a}_{\uparrow,n}^{\dagger}(0)$, and $\tilde{a}_{\downarrow,n}^{\dagger}(0)$ for the corresponding zero-momentum creation operators. We also write $\prod \tilde{a}^{\dagger}$ as shorthand for the product

$$\prod \tilde{a}^{\dagger} = \tilde{a}_{\uparrow,p}^{\dagger}(0) \tilde{a}_{\downarrow,p}^{\dagger}(0) \tilde{a}_{\uparrow,n}^{\dagger}(0) \tilde{a}_{\downarrow,n}^{\dagger}(0). \quad (44)$$

For the ground state energy calculations of ${}^3\text{H}$ and ${}^3\text{He}$ we use a lattice volume of $(16 \text{ fm})^3$. The initial states we choose are

$$|\Psi_i^{{}^3\text{H}}\rangle = \sum_{\mathbf{n}, \mathbf{n}', \mathbf{n}'', \mathbf{n}'''} e^{-\alpha|\mathbf{n}-\mathbf{n}'|} e^{-\alpha|\mathbf{n}-\mathbf{n}''|} e^{-\alpha|\mathbf{n}-\mathbf{n}'''} a_{\uparrow,p}^{\dagger}(\mathbf{n}') a_{\uparrow,n}^{\dagger}(\mathbf{n}'') a_{\downarrow,n}^{\dagger}(\mathbf{n}''') |0\rangle, \quad (45)$$

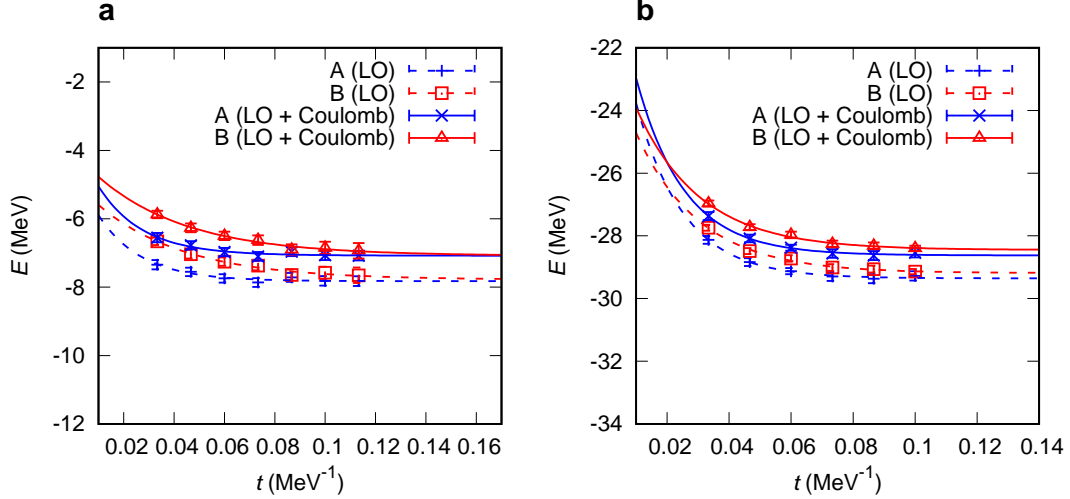
$$|\Psi_i^{{}^3\text{He}}\rangle = \sum_{\mathbf{n}, \mathbf{n}', \mathbf{n}'', \mathbf{n}'''} e^{-\alpha|\mathbf{n}-\mathbf{n}'|} e^{-\alpha|\mathbf{n}-\mathbf{n}''|} e^{-\alpha|\mathbf{n}-\mathbf{n}'''} a_{\uparrow,n}^{\dagger}(\mathbf{n}') a_{\uparrow,p}^{\dagger}(\mathbf{n}'') a_{\downarrow,p}^{\dagger}(\mathbf{n}''') |0\rangle, \quad (46)$$

with $\alpha = 2$ in lattice units. In panel **a** of Fig. 5 we show the energy versus projection time $t = L_t a_t$ for ${}^3\text{He}$ for the LO interaction A (blue plus signs and dashed lines), LO interaction B (red squares and dashed lines), LO + Coulomb interaction A (blue crosses and solid lines), and LO + Coulomb interaction B (red triangles and solid lines). As we are not including isospin-breaking effects other than Coulomb interactions, the LO and LO + Coulomb results for ${}^3\text{H}$ are exactly the same as the LO results for ${}^3\text{He}$. The error bars indicate one standard deviation errors due to the stochastic noise of the Monte Carlo simulations. The lines are extrapolations to infinite projection time using the ansatz,

$$E(t) = E_0 + c \exp[-\Delta E t], \quad (47)$$

where E_0 is the ground state energy that we wish to determine. The results for the ground state energies are shown in Table 1.

FIG. 5: Energy versus projection time for ${}^3\text{H}$, ${}^3\text{He}$, and ${}^4\text{He}$. In panels **a** and **b** we plot the energy versus projection time $t = L_t a_t$ for ${}^3\text{He}$ and ${}^4\text{He}$ respectively for the LO interaction A (blue plus signs and dashed lines), LO interaction B (red squares and dashed lines), LO + Coulomb interaction A (blue crosses and solid lines), and LO + Coulomb interaction B (red triangles and solid lines). The LO and LO + Coulomb results ${}^3\text{H}$ are the same as the LO results for ${}^3\text{He}$. The error bars indicate one standard deviation errors from the stochastic noise of the Monte Carlo simulations, and the lines show extrapolations to infinite projection time.



For the ground state energy calculations of ${}^4\text{He}$ we use a lattice volume of $(12 \text{ fm})^3$. The initial state we choose is

$$|\Psi_i^{4\text{He}}\rangle = \prod \tilde{a}^\dagger |0\rangle. \quad (48)$$

In panel **b** of Fig. 5 we show the energy versus projection time $t = L_t a_t$ for ${}^4\text{He}$ for the LO interaction A (blue plus signs and dashed lines), LO interaction B (red squares and dashed lines), LO + Coulomb interaction A (blue crosses and solid lines), and LO + Coulomb interaction B (red triangles and solid lines). The error bars indicate one standard deviation errors of the Monte Carlo simulations, and the lines are extrapolations to infinite projection time using the ansatz in Eq. (47). The results for the ground state energies are shown in Table 1.

We note that while that the ${}^3\text{H}$ energies for interactions A and B are underbound, the energies for ${}^4\text{He}$ are near the physical value. This may seem puzzling since in continuum-space calculations there is a well-known universal correlation between the ${}^3\text{H}$ and ${}^4\text{He}$ energies called the Tjon line [50–52]. Our lattice results show some deviation from this universal behavior due to lattice artifacts associated with our lattice spacing of 1.97 fm. This is not a new observation. The same behavior has been analyzed previously at the same lattice spacing but with a different lattice interaction [37, 53]. In order to match the physical ${}^3\text{H}$ and ${}^4\text{He}$ energies at the same time, higher-order short-range three-nucleon interactions at N^4LO and possibly the leading-order short-range four-nucleon interaction at N^5LO are needed. However a much simpler solution is to use a smaller lattice spacing, as these lattice deviations from the continuum-space Tjon line decrease very rapidly with the lattice spacing.

For the ground state energy calculations of ${}^8\text{Be}$, ${}^{12}\text{C}$, ${}^{16}\text{O}$, and ${}^{20}\text{Ne}$ we use a lattice volume of $(12 \text{ fm})^3$. The initial states we use are

$$|\Psi_i^{8\text{Be}}\rangle = \prod \tilde{a}^\dagger \cdot M_* \prod \tilde{a}^\dagger |0\rangle, \quad (49)$$

$$|\Psi_i^{12\text{C}}\rangle = \prod \tilde{a}^\dagger \cdot M_* \prod \tilde{a}^\dagger \cdot M_* \prod \tilde{a}^\dagger |0\rangle, \quad (50)$$

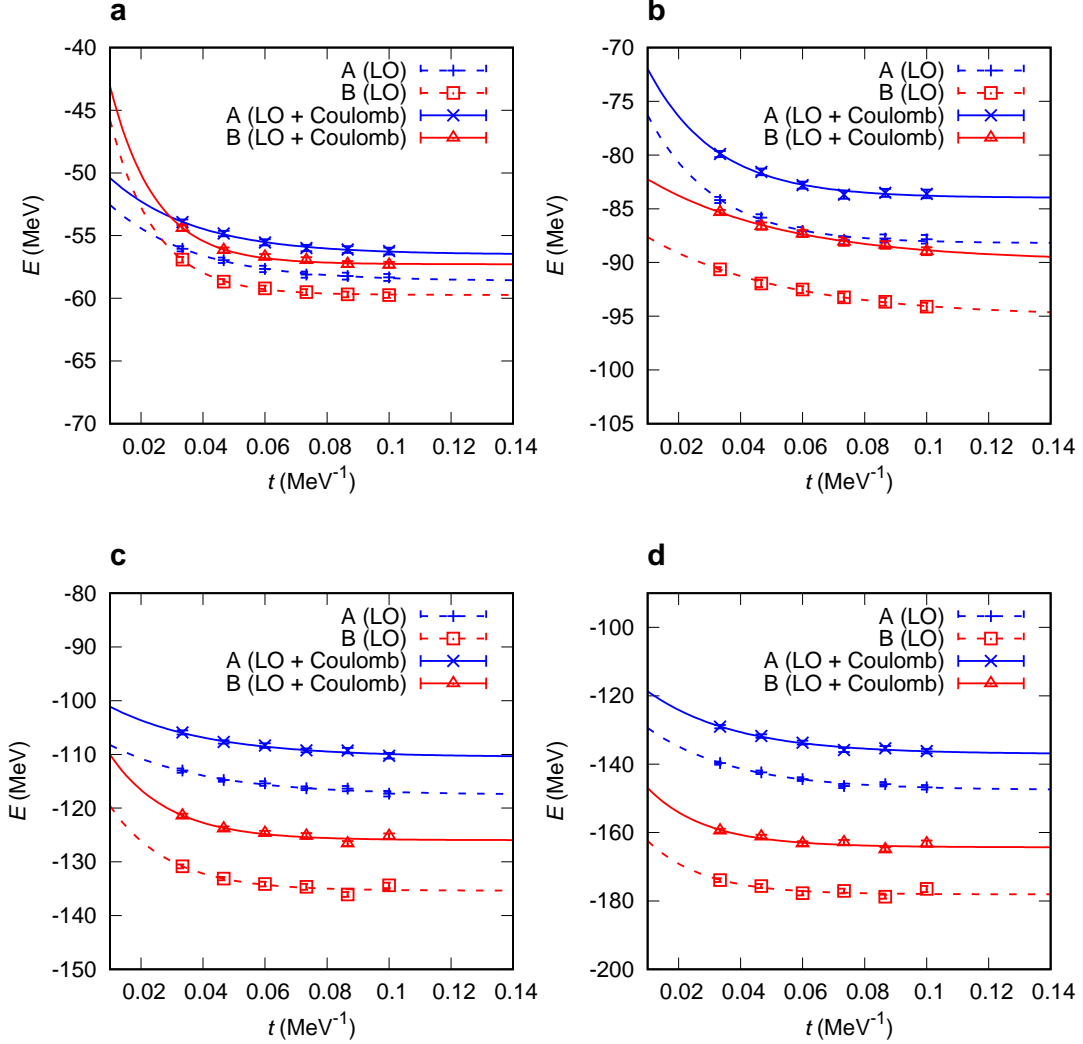
$$|\Psi_i^{16\text{O}}\rangle = \prod \tilde{a}^\dagger \cdot M_* \prod \tilde{a}^\dagger \cdot M_* \prod \tilde{a}^\dagger \cdot M_* \prod \tilde{a}^\dagger |0\rangle, \quad (51)$$

$$|\Psi_i^{20\text{Ne}}\rangle = \prod \tilde{a}^\dagger \cdot M_* \prod \tilde{a}^\dagger \cdot M_* \prod \tilde{a}^\dagger \cdot M_* \prod \tilde{a}^\dagger \cdot M_* \prod \tilde{a}^\dagger |0\rangle. \quad (52)$$

The interspersing of the transfer matrix M_* in between the products of creation operators allows us to create all nucleons with zero momentum without violating the Pauli exclusion principle. In panels **a**, **b**, **c**, **d** of Fig. 6 we show the energy versus projection time $t = L_t a_t$ for ${}^8\text{Be}$, ${}^{12}\text{C}$, ${}^{16}\text{O}$, and ${}^{20}\text{Ne}$ respectively for the LO interaction A (blue plus signs and dashed lines), LO interaction B (red squares and dashed lines), LO + Coulomb interaction A (blue

crosses and solid lines), and LO + Coulomb interaction B (red triangles and solid lines). The error bars indicate one standard deviation errors from the stochastic noise of the Monte Carlo simulations, and the lines are extrapolations to infinite projection time using the ansatz in Eq. (47). The results for the ground state energies are shown in Table 1.

FIG. 6: Energy versus projection time for ${}^8\text{Be}$, ${}^{12}\text{C}$, ${}^{16}\text{O}$, and ${}^{20}\text{Ne}$. In panels **a**, **b**, **c**, **d** we plot the energy versus projection time $t = L_t a t$ for ${}^8\text{Be}$, ${}^{12}\text{C}$, ${}^{16}\text{O}$, and ${}^{20}\text{Ne}$ respectively for the LO interaction A (blue plus signs and dashed lines), LO interaction B (red squares and dashed lines), LO + Coulomb interaction A (blue crosses and solid lines), and LO + Coulomb interaction B (red triangles and solid lines). The error bars indicate one standard deviation errors from the stochastic noise of the Monte Carlo simulations, and the lines show extrapolations to infinite projection time.



For both interactions A and B, the auxiliary-field Monte Carlo simulations presented here have far milder Monte Carlo sign cancellations than in previous lattice simulations of the same systems [11]. This very promising development will allow for much larger and previously difficult simulations in the future. The savings come from two innovations. The first is the introduction of the nonlocal interactions in V_{NL} . Ironically, the implementation of general nonlocal interactions in quantum Monte Carlo simulations have long been problematic due to sign oscillations. However, the auxiliary-field implementation of the interactions in V_{NL} are extremely favorable from the point of view of sign oscillations. The reason for this is the very simple structure of the terms in V_{NL} . This leads to fewer issues with so-called interference sign problems as discussed in Ref. [54]. The other innovation reducing the sign problem is the introduction of the parameter b_π in the one-pion exchange interaction. This decreases the short-distance repulsion in the S -wave channels responsible for some sign oscillations.

Adiabatic projection method

The adiabatic projection method is a general framework that produces a low-energy effective theory for clusters of particles which becomes exact in the limit of large projection time. The details of the methods used here were discussed in Ref. [18], and we review some of the main features here. On our L^3 periodic spatial lattice we consider a set of initial two-alpha states $|\mathbf{R}\rangle$ labeled by the spatial separation vector \mathbf{R} . For the alpha-alpha scattering calculations presented here we use $L = 16$ fm. The initial alpha wave functions are Gaussian wave packets which, for large $|\mathbf{R}|$, factorize as a product of two individual alpha clusters,

$$|\mathbf{R}\rangle = \sum_{\mathbf{r}} |\mathbf{r} + \mathbf{R}\rangle_1 \otimes |\mathbf{r}\rangle_2. \quad (53)$$

The summation over \mathbf{r} is required to produce states with total momentum equal to zero. As we have done in Eq. (23) for nucleon-nucleon scattering, we project onto spherical harmonics Y_{ℓ, ℓ_z} with angular momentum quantum numbers ℓ, ℓ_z ,

$$|R\rangle^{\ell, \ell_z} = \sum_{\mathbf{R}'} Y_{\ell, \ell_z}(\hat{\mathbf{R}}') \delta_{R, |\mathbf{R}'|} |\mathbf{R}'\rangle. \quad (54)$$

We only consider values for $|\mathbf{R}|$ less than $L/2$.

The next step is to multiply by powers of the transfer matrix to form dressed cluster states that approximately span the set of low-energy alpha-alpha scattering states in our periodic box. We start with the approximate transfer matrix M_* as in Eq. (30), and then follow with powers of the leading-order transfer matrix M . After n_t time steps, we have the dressed cluster states

$$|R\rangle_{n_t}^{\ell, \ell_z} = M^{n_t} M_*^{L_t} |R\rangle^{\ell, \ell_z}. \quad (55)$$

The dressed cluster states are then used to compute matrix elements of the transfer matrix M ,

$$[M_{n_t}]_{R', R}^{\ell, \ell_z} = \langle R' | M | R \rangle_{n_t}^{\ell, \ell_z}. \quad (56)$$

Since the states are not orthogonal, we compute a norm matrix

$$[N_{n_t}]_{R', R}^{\ell, \ell_z} = \langle R' | R \rangle_{n_t}^{\ell, \ell_z}. \quad (57)$$

The radial adiabatic transfer matrix is defined as the matrix product,

$$[M_{n_t}^a]_{R', R}^{\ell, \ell_z} = \left[N_{n_t}^{-\frac{1}{2}} M_{n_t} N_{n_t}^{-\frac{1}{2}} \right]_{R', R}^{\ell, \ell_z}. \quad (58)$$

Just as we have done for nucleon-nucleon scattering, we impose a spherical hard wall boundary at some radius R_W . For large n_t the standing waves of the radial adiabatic transfer matrix are used to determine the elastic phase shifts for alpha-alpha scattering. As explained in Ref. [18], this scattering calculation is extended out to very large volumes of $L^3 = (120 \text{ fm})^3$ using single alpha-particle simulations and including long-range Coulomb interactions between the otherwise non-interacting alpha particles at large distances.

In Fig. 7 we plot the LO + Coulomb S -wave phase shifts for interaction A at several laboratory energies versus the number of time steps $L_t = 2n_t + 1$. The analogous LO + Coulomb S -wave phase shifts for interaction B are shown in Fig. 8. For both of these figures, the panels **a**, **b**, **c**, **d**, **e**, **f**, **g** correspond to laboratory energies $E_{\text{Lab}} = 1.0, 2.0, 3.0, 4.5, 6.5, 8.5, 10.0$ MeV respectively. The error bars indicate one standard deviation uncertainties due to Monte Carlo errors, and the dot-dashed lines show the extrapolation curve for the $L_t \rightarrow \infty$ limit. We use the ansatz

$$\delta_0(L_t, E) = \delta_0(E) + c_0(E) \exp[-\Delta E L_t a_t], \quad (59)$$

where $\delta_0(E)$ is the extrapolated phase shift. The hatched regions in Fig. 7 and 8 show the one standard deviation error estimate of the extrapolation.

Tight-binding approximation and potential

The tight-binding approximation is a simple qualitative picture where the alpha particle is treated as a compact object with a small but nonzero radius, R_α . As the name suggests, it is conceptually similar to the tight-binding

FIG. 7: Alpha-alpha S -wave extrapolations for interaction A. LO + Coulomb results (circles) for the S -wave phase shift for interaction A at several laboratory energies versus the number of time steps $L_t = 2n_t + 1$. The panels **a**, **b**, **c**, **d**, **e**, **f**, **g** correspond to laboratory energies $E_{\text{Lab}} = 1.0, 2.0, 3.0, 4.5, 6.5, 8.5, 10.0$ MeV respectively. The error bars indicate one standard deviation uncertainty due to Monte Carlo errors. The dot-dashed lines show the extrapolation to the $L_t \rightarrow \infty$ limit, and the hatched regions show the one standard deviation error estimate for the extrapolation.

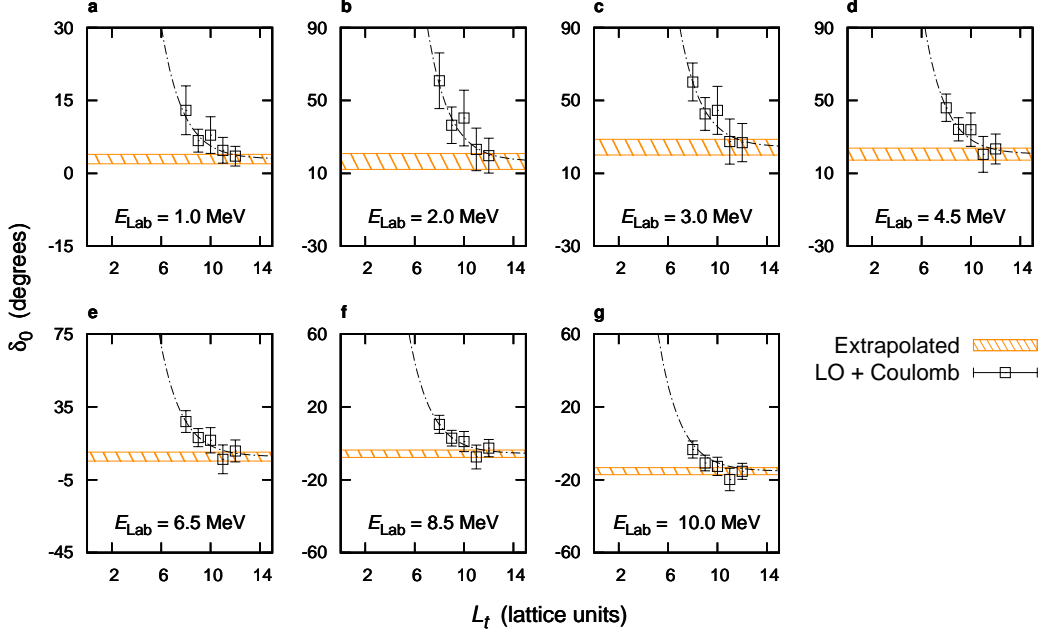
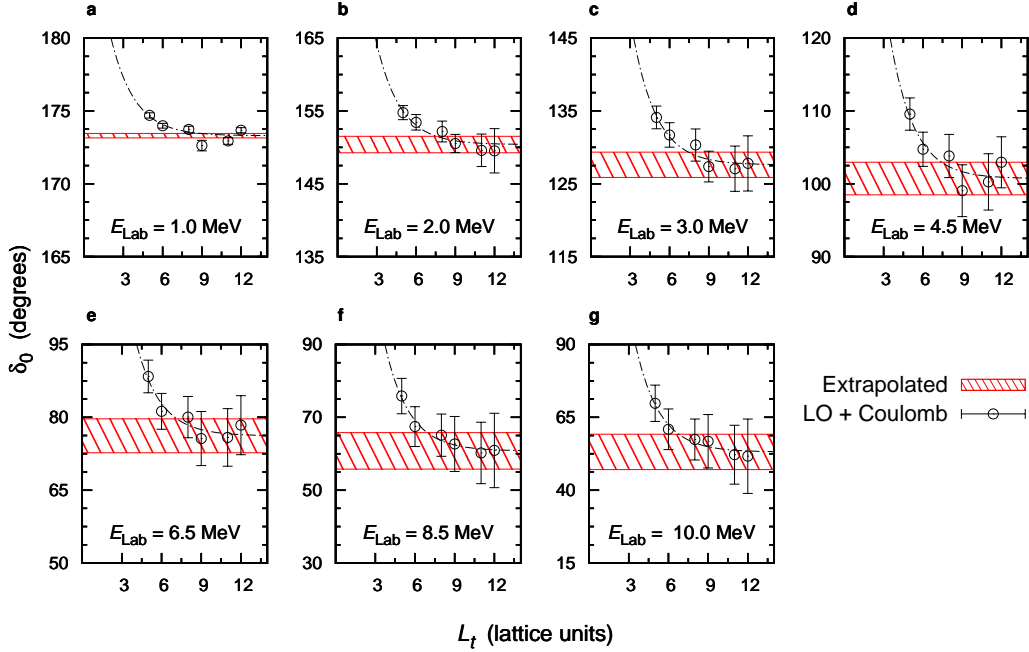


FIG. 8: Alpha-alpha S -wave extrapolations for interaction B. LO + Coulomb results (circles) for the S -wave phase shift for interaction B at several laboratory energies versus the number of time steps $L_t = 2n_t + 1$. The panels **a**, **b**, **c**, **d**, **e**, **f**, **g** correspond to laboratory energies $E_{\text{Lab}} = 1.0, 2.0, 3.0, 4.5, 6.5, 8.5, 10.0$ MeV respectively. The error bars indicate one standard deviation uncertainty due to Monte Carlo errors. The dot-dashed lines show the extrapolation to the $L_t \rightarrow \infty$ limit, and the hatched regions show the one standard deviation error estimate for the extrapolation.



model of electronic structure commonly used in condensed matter physics. Here we provide some further details of the direct and exchange terms in the calculation of the tight-binding potential between two alpha clusters. Let us consider a nucleon-nucleon interaction in continuous space of the form

$$\frac{1}{2} \int d^3\mathbf{R} d^3\mathbf{r}' d^3\mathbf{r} V_{s_4, i_4; s_3, i_3}^{s_2, i_2; s_1, i_1}(\mathbf{r}', \mathbf{r}) a_{s_3, i_3}^\dagger(\mathbf{R} - \mathbf{r}'/2) a_{s_4, i_4}^\dagger(\mathbf{R} + \mathbf{r}'/2) a_{s_2, i_2}(\mathbf{R} + \mathbf{r}/2) a_{s_1, i_1}(\mathbf{R} - \mathbf{r}/2). \quad (60)$$

The indices s_1, s_2, s_3, s_4 correspond to spin, while i_1, i_2, i_3, i_4 correspond to isospin. For $r > R_\alpha$, the tight-binding potential $V_{\text{TB}}(r)$ can be divided into two contributions,

$$V_{\text{TB}}(r) = V_{\text{TB}}^{\text{direct}}(r) + V_{\text{TB}}^{\text{exchange}}(r), \quad (61)$$

where the direct term is

$$V_{\text{TB}}^{\text{direct}}(|\mathbf{r}|) = \sum_{s_{24}, i_{24}} \sum_{s_{13}, i_{13}} \int_{|\mathbf{r}' - \mathbf{r}| < R_\alpha} d^3\mathbf{r}' V_{s_{24}, i_{24}; s_{13}, i_{13}}^{s_{24}, i_{24}; s_{13}, i_{13}}(\mathbf{r}', \mathbf{r}), \quad (62)$$

and the exchange term is

$$V_{\text{TB}}^{\text{exchange}}(|\mathbf{r}|) = - \sum_{s_{23}, i_{23}} \sum_{s_{14}, i_{14}} \int_{|\mathbf{r}' + \mathbf{r}| < R_\alpha} d^3\mathbf{r}' V_{s_{14}, i_{14}; s_{23}, i_{23}}^{s_{23}, i_{23}; s_{14}, i_{14}}(\mathbf{r}', \mathbf{r}). \quad (63)$$

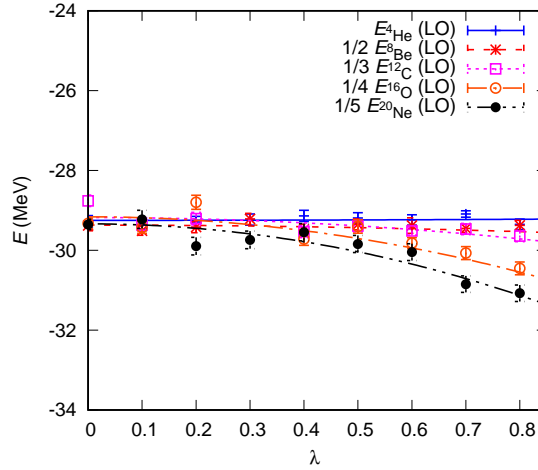
Ground state energies as a function of λ

We consider the one-parameter family of interactions, $V_\lambda = (1 - \lambda)V_A + \lambda V_B$ with the Coulomb interactions switched off. At the phase transition point the alpha clusters become non-interacting in the dilute limit, and so we should find the following simple relationship among the ground state energies provided that the finite volume is sufficiently large:

$$E_{4\text{He}} = 1/2 E_{8\text{Be}} = 1/3 E_{12\text{C}} = 1/4 E_{16\text{O}} = 1/5 E_{20\text{Ne}}. \quad (64)$$

In Fig. 9 we plot the LO ground state energies $E_{4\text{He}}, 1/2 E_{8\text{Be}}, 1/3 E_{12\text{C}}, 1/4 E_{16\text{O}}, 1/5 E_{20\text{Ne}}$ versus λ . We see that the phase transition occurs at $\lambda_\infty = 0.0(1)$.

FIG. 9: Ground state energies versus λ . We plot the LO ground state energies $E_{4\text{He}}, 1/2 E_{8\text{Be}}, 1/3 E_{12\text{C}}, 1/4 E_{16\text{O}}, 1/5 E_{20\text{Ne}}$ versus the parameter λ which interpolates between V_A and V_B .



To determine the critical point λ_{20} when ^{20}Ne becomes bound, we compare $E_{20\text{Ne}}$ with the threshold energy $E_{16\text{O}} + E_{4\text{He}}$. For this analysis we also include the finite-volume energy one obtains at infinite S -wave scattering length for the $^{16}\text{O} + ^4\text{He}$ system. At infinite scattering length the energy of any two-body system with reduced mass μ in a periodic box of size L is [55, 56]

$$\Delta E = \frac{4\pi^2 d_1}{mL^2}, \quad (65)$$

where

$$d_1 \approx -0.095901. \quad (66)$$

We find that the critical point for the binding of ^{20}Ne is $\lambda_{20} = 0.2(1)$. A similar analysis for the binding of the other alpha nuclei finds $\lambda_{16} = 0.2(1)$ for ^{16}O , $\lambda_{12} = 0.3(1)$ for ^{12}C , and $\lambda_8 = 0.7(1)$ for ^8Be .

Code Availability

All codes used in this work are freely available and can be obtained by contacting the authors.

-
- [1] Y. Funaki, A. Tohsaki, H. Horiuchi, P. Schuck, and G. Röpke, *Phys. Rev.* **C67**, 051306 (2003), nucl-th/0302017.
- [2] M. Chernykh, H. Feldmeier, T. Neff, P. von Neumann-Cosel, and A. Richter, *Phys. Rev. Lett.* **98**, 032501 (2007).
- [3] E. Epelbaum, H. Krebs, D. Lee, and U.-G. Meißner, *Phys. Rev. Lett.* **106**, 192501 (2011), arXiv:1101.2547 [nucl-th].
- [4] W. R. Zimmerman, N. E. Destefano, M. Freer, M. Gai, and F. D. Smit, *Phys. Rev. C* **84**, 027304 (2011).
- [5] E. Epelbaum, H. Krebs, T. Lähde, D. Lee, and U.-G. Meißner, *Phys. Rev. Lett.* **109**, 252501 (2012), 1208.1328.
- [6] A. C. Dreyfuss, K. D. Launey, T. Dytrych, J. P. Draayer, and C. Bahri, *Phys. Lett.* **B727**, 511 (2013), 1212.2255.
- [7] V. N. Efimov, *Sov. J. Nucl. Phys.* **12**, 589 (1971).
- [8] E. Braaten and H.-W. Hammer, *Phys. Rept.* **428**, 259 (2006).
- [9] R. Roth, J. Langhammer, A. Calci, S. Binder, and P. Navratil, *Phys. Rev. Lett.* **107**, 072501 (2011), 1105.3173.
- [10] H. Hergert, S. K. Bogner, S. Binder, A. Calci, J. Langhammer, R. Roth, and A. Schwenk, *Phys. Rev.* **C87**, 034307 (2013), 1212.1190.
- [11] T. A. Lähde, E. Epelbaum, H. Krebs, D. Lee, U.-G. Meißner, and G. Rupak, *Phys. Lett.* **B732**, 110 (2014), 1311.0477.
- [12] V. Soma, C. Barbieri, and T. Duguet, *Phys. Rev.* **C89**, 024323 (2014), 1311.1989.
- [13] J. Carlson, S. Gandolfi, F. Pederiva, S. C. Pieper, R. Schiavilla, K. E. Schmidt, and R. B. Wiringa (2014), 1412.3081.
- [14] J. Simonis, K. Hebeler, J. D. Holt, J. Menendez, and A. Schwenk, *Phys. Rev.* **C93**, 011302 (2016), 1508.05040.
- [15] G. Hagen et al., *Nature Phys.* (2015), 1509.07169.
- [16] E. Epelbaum, H.-W. Hammer, and U.-G. Meißner, *Rev. Mod. Phys.* **81**, 1773 (2009), arXiv:0811.1338 [nucl-th].
- [17] S. A. Afzal, A. A. Z. Ahmad, and S. Ali, *Rev. Mod. Phys.* **41**, 247 (1969).
- [18] S. Elhatisari, D. Lee, G. Rupak, E. Epelbaum, H. Krebs, T. A. Lähde, T. Luu, and U.-G. Meißner, *Nature* **528**, 111 (2015), 1506.03513.
- [19] W. N. Polyzou and W. Glöckle, *Few-Body Syst.* **9**, 97 (1990).
- [20] S. K. Bogner, R. J. Furnstahl, and R. J. Perry, *Phys. Rev.* **C75**, 061001 (2007), nucl-th/0611045.
- [21] G. Imbriani, M. Limongi, L. Gialanella, F. Terrasi, O. Straniero, A. Chieffi, and O. A. d. Roma, *Astrophys. J.* **558**, 903 (2001), astro-ph/0107172.
- [22] P. Maris, J. P. Vary, and A. M. Shirokov, *Phys. Rev.* **C79**, 014308 (2009), arXiv:0808.3420 [nucl-th].
- [23] A. Ekström, G. R. Jansen, K. A. Wendt, G. Hagen, T. Papenbrock, B. D. Carlsson, C. Forssen, M. Hjorth-Jensen, P. Navratil, and W. Nazarewicz, *Phys. Rev.* **C91**, 051301 (2015), 1502.04682.
- [24] E. Ruiz Arriola (2007), 0709.4134.
- [25] H. T. C. Stoof, *Phys. Rev. A* **49**, 3824 (1994), cond-mat/9402041.
- [26] Y. Kagan, A. E. Muryshev, and G. V. Shlyapnikov, *Physical Review Letters* **81**, 933 (1998), cond-mat/9801168.
- [27] T. Kraemer, M. Mark, P. Waldburger, J. G. Danzl, C. Chin, B. Engeser, A. D. Lange, K. Pilch, A. Jaakkola, H.-C. Naegerl, et al., *Nature* **440**, 315 (2006), cond-mat/0512394.
- [28] E. Epelbaum, H. Krebs, T. A. Lähde, D. Lee, U.-G. Meißner, and G. Rupak, *Phys. Rev. Lett.* **112**, 102501 (2014), 1312.7703.
- [29] H. W. Hammer and L. Platter, *Eur. Phys. J.* **A32**, 113 (2007), nucl-th/0610105.
- [30] J. von Stecher, J. P. D’Incao, and C. H. Greene, *Nat Phys* **5**, 417 (2009).
- [31] J. A. Wheeler, *Phys. Rev.* **52**, 1083 (1937).
- [32] D. M. Dennison, *Phys. Rev.* **96**, 378 (1954).
- [33] J. W. Clark and T.-P. Wang, *Ann. Phys.* **40**, 127 (1966).
- [34] D. Robson, *Phys. Rev. Lett.* **42**, 876 (1979).
- [35] W. Bauhoff, H. Schultheis, and R. Schultheis, *Phys. Rev.* **C29**, 1046 (1984).
- [36] A. Tohsaki, H. Horiuchi, P. Schuck, and G. Röpke, *Phys. Rev. Lett.* **87**, 192501 (2001), nucl-th/0110014.
- [37] E. Epelbaum, H. Krebs, D. Lee, and U.-G. Meißner, *Eur. Phys. J.* **A45**, 335 (2010), arXiv:1003.5697 [nucl-th].
- [38] N. Klein, D. Lee, W. Liu, and U.-G. Meißner, *Phys. Lett.* **B747**, 511 (2015), 1505.07000.
- [39] J. Carlson, V. Pandharipande, and R. Wiringa, *Nucl. Phys. A* **424**, 47 (1984), ISSN 0375-9474, URL <http://www.sciencedirect.com/science/article/pii/0375947484901271>.
- [40] B. Borasoy, E. Epelbaum, H. Krebs, D. Lee, and U.-G. Meißner, *Eur. Phys. J.* **A34**, 185 (2007), arXiv:0708.1780 [nucl-th].
- [41] B.-N. Lu, T. A. Lähde, D. Lee, and U.-G. Meißner (2015), 1506.05652.

- [42] V. G. J. Stoks, R. A. M. Kompl, M. C. M. Rentmeester, and J. J. de Swart, *Phys. Rev.* **C48**, 792 (1993).
- [43] E. Wigner, *Phys. Rev.* **51**, 106 (1937).
- [44] J.-W. Chen, D. Lee, and T. Schäfer, *Phys. Rev. Lett.* **93**, 242302 (2004), nucl-th/0408043.
- [45] D. Lee, *Phys. Rev. Lett.* **98**, 182501 (2007), nucl-th/0701041.
- [46] D. Lee, *Prog. Part. Nucl. Phys.* **63**, 117 (2009), arXiv:0804.3501 [nucl-th].
- [47] J. Hubbard, *Phys. Rev. Lett.* **3**, 77 (1959).
- [48] R. L. Stratonovich, *Soviet Phys. Doklady* **2**, 416 (1958).
- [49] S. E. Koonin, *Journal of Statistical Physics* **43**, 985 (1986), ISSN 0022-4715, URL <http://dx.doi.org/10.1007/BF02628325>.
- [50] J. Tjon, *Physics Letters B* **56**, 217 (1975), ISSN 0370-2693, URL <http://www.sciencedirect.com/science/article/pii/0370269375903780>.
- [51] A. Nogga, H. Kamada, and W. Gloeckle, *Phys. Rev. Lett.* **85**, 944 (2000), nucl-th/0004023.
- [52] L. Platter, H.-W. Hammer, and U.-G. Meißner, *Phys. Lett.* **B607**, 254 (2005), nucl-th/0409040.
- [53] E. Epelbaum, H. Krebs, D. Lee, and U.-G. Meißner, *Phys. Rev. Lett.* **104**, 142501 (2010), arXiv:0912.4195 [nucl-th].
- [54] T. A. Lähde, T. Luu, D. Lee, U.-G. Meißner, E. Epelbaum, H. Krebs, and G. Rupak, *Eur. Phys. J.* **A51**, 92 (2015), 1502.06787.
- [55] D. Lee, *Phys. Rev.* **B73**, 115112 (2006), cond-mat/0511332.
- [56] S. R. Beane, P. F. Bedaque, A. Parreno, and M. J. Savage, *Phys. Lett.* **B585**, 106 (2004), hep-lat/0312004.